



1 **iFit: An intensity-based retrieval for SO₂ and BrO from scattered sunlight**
2 **ultraviolet volcanic plume absorption spectra**

3
4 M.R. Burton^{1,*} and G.M. Sawyer²

5
6 1. School of Earth and Environment, University of Manchester, Manchester, UK
7 2. Laboratoire Magmas et Volcans, Université Blaise Pascal, Clermont Ferrand,
8 France

9
10 *Corresponding author : mike.burton@manchester.ac.uk

11
12
13 **Abstract**

14

15 iFit is a new intensity-based retrieval algorithm for direct fitting of measured UV
16 spectra, specifically developed for use in volcanology. It has been designed with a
17 focus on minimising processing of the measured spectra prior to analysis. Here, we
18 report a detailed presentation of the iFit algorithm, and test it in 4 case studies,
19 examining clear sky spectra, SO₂ calibration cell experiments and volcanic SO₂ and
20 BrO retrievals from traverse measurements performed on Mt. Etna volcano, Italy.

21

22 We show that the major source of fit error in the intensity fitting come from air mass
23 factor independent solar spectrum errors, which are, however, easily characterised and
24 removed by dividing the measured spectrum by a pre-calculated solar spectrum
25 residual. Furthermore, we have quantified the magnitude of the flat spectrum in two
26 spectrometers, and shown that this spectrum is strongly spectrometer dependent but
27 temperature independent, opening the possibility for robust analysis and
28 quantification of both SO₂ and BrO without the need for temperature stabilisation of
29 the spectrometer.

30



31 We find that iFit can be robustly and easily applied to traverse measurements of
32 volcanic plumes, producing bias-free profiles of SO₂, and high quality SO₂/BrO ratios
33 without the need for clear sky background spectra. Fit residuals are typically pure
34 instrumental noise when the residual solar spectrum is removed.

35 We believe that the iFit approach, which avoids the need for a clear sky spectrum and
36 which achieves noise-limited fits, is ideally suited to the automated analysis of spectra
37 produced by networks of scanning UV spectrometers around volcanoes.

38

39 Keywords: SO₂, volcanic gas, DOAS, UV spectroscopy, iFit

40

41 **1. Introduction**

42

43 The introduction of the USB2000 spectrometer (Galle et al., 2003) revolutionised the
44 measurement of SO₂ fluxes in volcanology. The direct measurement of a spectrum
45 allowed much more sophisticated analysis compared with the “black box” of the
46 previously used COSPEC (Stoiber and Jepsen, 1973). Analysis of USB2000 spectra
47 using differential optical absorption (DOAS) techniques (Platt and Stutz, 2008)
48 rapidly became the standard approach for retrieval of SO₂. The detection and
49 quantification of BrO in USB2000 spectra using the DOAS technique (Bobrowski et
50 al., 2003) further cemented the association between the instrument and the retrieval
51 approach, such that many groups began referring to the instrument by the analysis
52 technique, e.g. mini-DOAS spectrometer. The flexibility of the USB2000
53 spectrometer and associated optics opened the possibility of arrays of scanning
54 spectrometers arranged around volcanoes, permitting automatic, real-time monitoring
55 of SO₂ fluxes. This led to the installation of such networks, first on Montserrat



56 (Edmonds et al., 2003), then on Etna and Stromboli (e.g., Burton et al., 2009; Salerno
57 et al., 2009a, b), and later on over 20 volcanoes worldwide as part of the NOVAC
58 project (Galle et al., 2010).

59

60 In this work we present a novel retrieval methodology for volcanic SO₂ and BrO from
61 UV spectra, which we call “iFit” for intensity-fitting. We use an intensity-based
62 approach in which we attempt to directly simulate and fit the measured spectrum as it
63 is, with very limited manipulation of original data. The forward model is capable of
64 calculating a UV spectrum from first principles, following the physical processes
65 arising from radiative transfer and instrumental effects which produce the measured
66 spectrum. The main initial motivation for the development of this approach was to
67 avoid the requirement of the DOAS methodology of a measured ‘clear-sky’ reference
68 spectrum, which can at times be impossible to measure from a fixed array because the
69 plume is so wide that no clear sky spectra are available. Performing a DOAS analysis
70 with a reference spectrum which includes an unknown amount of SO₂ results in an
71 unknown bias in the measured SO₂ amounts; on the contrary, our approach does not
72 require a measured reference spectrum, and therefore we can be confident systematic
73 biases in SO₂ content are not present. In other words, using iFit we can be sure zero is
74 actually zero on our SO₂ scale.

75

76 Apart from the advantages of a calculated clear-sky spectrum, there are also several
77 inherent advantages of an intensity-based technique. These include automatic
78 inclusion of the I₀ effect (Aliwell et al., 2002), thanks to a high resolution version of
79 the solar spectrum. The intensity retrieval also allows quantification of the broad
80 absorption produced by the presence of particulates. Furthermore, inclusion of light-



81 dilution effects is direct, and this will be investigated in more detail in a future paper.
82 Finally, as we show in the case studies below, the SO₂ absorption itself has a large
83 broadband component that is removed in the DOAS approach, but which contains
84 useful information that aids in the intensity fitting procedure.

85

86 In the following sections we briefly review the DOAS approach, and describe a
87 hybrid retrieval which is currently in use on Etna and Stromboli scanning networks.
88 We then explain the iFit methodology in detail. We present case studies from clear
89 sky spectra, calibration cell spectra and traverse measurements on Mt. Etna (Sicily,
90 Italy). We then discuss the results from the case studies and conclude by examining
91 new frontiers which are opened using the novel retrieval technique.

92

93 **2. Volcanic Plume SO₂ and BrO Retrieval Methodologies**

94

95 The most widely used volcanic plume SO₂ and BrO retrieval methodologies are based
96 around the DOAS technique (Platt and Stutz, 2008). The DOAS technique consists of
97 taking a measurement spectrum and a clear sky spectrum and dividing them to
98 produce a transmittance spectrum. This is then converted to optical depth by taking
99 the negative natural log of the transmittance. The optical depth spectrum is then
100 normalised by dividing with a smooth polynomial fitted to the optical depth spectrum:

101

$$102 \text{ DOAS spectrum} = (-\ln(I_m/I_{\text{sky}})) / \text{poly}[-\ln(I_m/I_{\text{sky}})] \quad 1.$$

103

104 Where I_m is the measured intensity spectrum, I_{sky} is the measured clear sky spectrum
105 and $\text{poly}[]$ is a polynomial fit.



106

107 The resulting spectrum is therefore a differential optical depth spectrum, hence the
108 DOAS name. By applying the same normalisation to calculated optical depth spectra
109 the DOAS spectrum can be simply and, for weak lines, linearly fitted. Differential
110 optical depths significantly greater than 0.1 demonstrate a non-linear relationship with
111 increasing gas amount due to Beer's law:

112

$$113 \quad t = I_m/I_{sky} = \exp(-\tau) = \exp(-\text{path_amount} \cdot \text{absorption coefficient}) \quad 2.$$

114

115 where τ is the optical depth, and t the transmittance. The Taylor expansion of $\exp(-\tau)$
116 is

$$117 \quad 1 - \tau + (\tau^2/2) - (\tau^3/6) \dots \quad 3.$$

118

119 So it is clear that when τ is less than ~ 0.1 , $(\tau^2/2)$ and higher orders are small and $\exp(-$
120 $\tau)$ approximates to the linear relationship $1-\tau$. SO_2 abundances in volcanic plumes are
121 often significantly greater than 0.1, and therefore more sophisticated techniques are
122 required.

123

124 In order to accurately calculate optical depth spectra to fit to the measured DOAS
125 spectrum we must first take account of the instrument lineshape (ILS) of our
126 spectrometer, if the resolution of the spectrometer is too low to fully resolve the
127 natural absorption lines, which is typically the case. Since raw spectra are measured in
128 intensity, the convolution of the ILS with the measurement must also be performed in
129 terms of intensity. Therefore, the correct procedure for the calculation of optical depth
130 spectra to be fitted to the measured DOAS spectrum is to calculate a transmittance



131 spectrum by multiplying an absorption cross-section of the desired gas with the
132 estimated gas amount in the spectrum, convolve this transmittance spectrum with the
133 ILS, convert to optical depth by taking the negative natural log and then normalise
134 with a fitted polynomial:

135

$$136 \text{ gas_}\tau = -\ln(\text{ILS} \otimes (\exp(-\text{amt.xsec}))) / \text{poly}[-\ln(\text{ILS} \otimes (\exp(-\text{amt.xsec})))] \quad 4.$$

137

138 Where $\text{gas_}\tau$ is the calculated optical depth spectrum to be used in the DOAS fit, \otimes
139 represents a convolution, amt is the path amount of gas, and xsec is that gas's
140 absorption cross-section.

141

142 It is important to note that:

143

$$144 -\ln(\text{ILS} \otimes (\exp(-\text{amt.xsec.n})) \neq n \cdot (-\ln(\text{ILS} \otimes (\exp(-\text{amt.xsec}))) \quad 5.$$

145

146 Where n is an arbitrary multiplication factor. In other words, when the gas amount
147 changes a new transmittance spectrum must be calculated and reconvolved with the
148 ILS; simply multiplying the optical depth spectrum by a factor will not produce the
149 same, physically realistic, result.

150

151 It is therefore clear that the correct application of the DOAS approach requires that all
152 calculations of fitted spectra are performed first in transmittance (intensity) and then
153 converted to optical depth each iteration. The question we pose is: if we are
154 performing the calculations of transmittance in terms of intensity, why not perform
155 the fit in terms of intensity as well?



156

157 Direct fitting of measured intensities is, in fact, frequently used for analysis of UV
158 spectra. The Global Ozone Monitoring Experiment (GOME) is analysed with such a
159 method (Van Roozendael et al., 2012). In their analysis they find significant
160 advantages for the direct fitting approach over DOAS, which neglects the wavelength
161 dependency of the photon path length, producing misfits in ozone retrievals.

162

163 We chose the direct fitting approach of iFit for three main reasons. Firstly, it avoids
164 the requirement for a clear sky spectrum, thus greatly enhancing the flexibility and
165 applicability of the retrieval. Secondly, in principle the fewer manipulations (i.e.
166 converting to optical depth) of the raw spectrum the better, as with each manipulation
167 there is the possibility to introduce errors. Finally, since the SO₂ fit is performed on
168 the edge of a strong ozone absorption band there are low intensities at low solar zenith
169 angles. In the DOAS approach this can lead to very large numbers in the DOAS
170 spectrum, as clear sky spectra contain numbers close to zero. In the direct fitting
171 approach there is no such division by small numbers, and the low intensity is
172 manifested as an easy to manage increase in noise levels.

173

174 The DOAS retrieval is used both by NOVAC (Galle et al., 2010) and in the recently
175 published SO₂ retrieval suite by Kantzas et al. (2012). In both cases clear sky spectra
176 are required, limiting their applicability.

177

178 A hybrid direct-fitting DOAS approach was developed for the analysis of UV spectra
179 collected with the FLAME (Flux Automatic MEasurement) network on Mt. Etna and
180 Stromboli (Salerno et al. 2009a, b). This worked in differential optical depth, but



181 included the Fraunhofer spectrum in order to avoid the need for a clear sky spectrum.
182 The retrieval was investigated thoroughly and judged to be suitable for the automatic
183 analysis of UV spectra produced by the FLAME networks (Salerno et al, 2009b).

184

185 Here we show that a fully direct intensity fit can produce robust results without the
186 need for clear sky spectra. In the following sections we describe the iFit retrieval in
187 detail, and apply it to several case studies, demonstrating its potential in the field of
188 volcanology.

189

190 **3. The Ocean Optics USB2000 and USB2000+ spectrometers**

191

192 While the iFit retrieval can in principle be applied to any UV spectrum, it has been
193 developed with a specific focus on analysing spectra produced by the Ocean Optics
194 (www.oceanoptics.com) USB2000 family of spectrometers. These spectrometers are
195 currently the default tool for volcanologists measuring SO₂ fluxes, thanks to their
196 reasonable cost, robustness and ease of use. The spectrometers are illuminated with a
197 fibre optic cable connected to a quartz collimator. Light enters the spectrometer
198 through a vertical slit and illuminates a diffraction grating. The wavelength-sorted
199 light then passes through focussing elements and optional filters before being detected
200 with a 2048-element horizontal CCD. Three elements of this system are of particular
201 relevance for the iFit retrieval. Firstly, the form of the instrument lineshape (ILS) is
202 determined by the entrance slit, and can be modelled through a combination of a
203 Gaussian-boxcar combination, with greater boxcar contribution with increasing slit
204 width. The slit width is fixed when the spectrometer is manufactured, and there are a
205 variety of different widths available, from 25 micron to 200 micron. Accurate



206 representation of the ILS is essential for producing good quality fits. This is achieved
207 in iFit by directly fitting the width of the ILS during the retrieval, and manually
208 adjusting the relative weight of Gaussian and boxcar forms until optimal fitting is
209 achieved.

210

211 The second group of critical instrumental effects that must be addressed are dark
212 current, bias and stray light. From the moment that charges are read out from the CCD,
213 emptying the charge wells, electrons begin to accumulate at a rate which is both pixel-
214 dependent and temperature dependent. This signal is called the dark current, and it is a
215 ubiquitous process, continuing whether the CCD is illuminated or not. In typical well-
216 illuminated situations the dark current is insignificant (less than 1 part per mil)
217 compared with the measured signals, but in poorly illuminated cases it can become
218 significant. The bias signal is the nominal ‘zero’ intensity level for the CCD, and is
219 determined by the CCD electronic configuration and temperature. On the USB2000
220 spectrometers the bias level is inversely proportional to temperature, and at high
221 temperatures the bias level may even fall below zero. For a thermo-stabilised
222 instrument the dark current and bias can be removed from measured spectra by
223 subtracting a dark spectrum, which is collected with the same exposure time and
224 number of coadds as measured spectra, but with the CCD unilluminated.

225

226 Stray light can be produced by any photons which are scattered within the body of the
227 spectrometer, producing a close-to-flat offset in addition to the bias. This effect can be
228 greatly reduced through the use of a short-pass filter, which eliminates wavelengths
229 greater than those required for SO₂ and BrO retrievals, typically those longer than 400
230 nm. USB2000’s can be ordered with such an optional short-pass filter. In practice, the



231 effect of stray light is observed as a residual positive offset in parts of the spectrum in
232 which no light should be present, below 300 nm. It is therefore essential to include
233 ~20 nm of the spectrum below 300 nm when specifying the USB2000 spectrometer in
234 order to correctly characterise the stray light signal. It can then be removed by taking
235 the average of a section of the unilluminated spectrum below 300 nm and subtracting
236 this value from the whole spectrum.

237

238 The third instrumental effect of note is the flat spectrum, produced by small pixel-to-
239 pixel variations in the conversion rate of photons to electrons in the CCD array. We
240 have characterised this effect by illuminating a spectrometer with broadband light
241 from a deuterium lamp (Ocean Optics model DT1000) and dividing the resulting
242 spectrum with a polynomial fit. The amplitude and structure of the flat spectrum
243 varies significantly from one spectrometer to another but for a given spectrometer it
244 appears to be temperature independent (Figure 1). Note that when a measured clear
245 sky spectrum is used in the DOAS approach the flat spectrum is automatically
246 removed. Instead, for iFit it must be accurately characterised, either via direct
247 measurement or inclusion of the retrieval residual. Because it is pixel dependent it is
248 not affected by wavelength shifts, and therefore may affect clear sky spectrum
249 corrected DOAS retrievals if the spectrometer temperature changes after the clear sky
250 spectrum is collected.

251

252 A final ubiquitous characteristic of CCD detectors is noise. There are two main
253 sources of noise, read noise and shot noise. Read noise is produced upon read-out,
254 amplification and analogue-to-digital conversion of the accumulated charge in each
255 pixel of the CCD. Shot noise is an inherent characteristic of the particle nature of light,



256 with individual photons producing charge in each pixel. It follows Poisson statistics,
257 and is therefore proportional to the square-root of the recorded digital counts. In well-
258 illuminated situations shot noise dominates read noise in the USB2000. As we will
259 demonstrate, the empirically derived measurement error is typically equivalent to the
260 fit error, producing a fit residual which consists purely of instrumental noise.

261

262 **4. The iFit algorithm**

263

264 **4.1 Pre-analysis procedures applied to the measured spectra**

265

266 A specific objective of the iFit approach is to manipulate the measured spectra as little
267 as possible, in order to avoid unintended side-effects in the retrieval. To this end the
268 only procedures applied to the measured spectra prior to analysis were removal of the
269 dark spectrum (if available), removal of the stray light effect, and division of the
270 resulting spectrum by the previously measured flat spectrum (if available). Flat
271 spectrum removal is performed in the pre-analysis stage because of the fixed pixel
272 nature of the flat spectrum, which means it is unaffected by wavelength shifts, which
273 are applied later in the forward model.

274

275 A final step in the pre-analysis procedure is to determine the measurement error (see
276 section 4.5).

277

278 **4.2 The iFit forward model**

279



280 Armed with a thorough understanding of instrumental effects we may now consider
281 the radiative transfer processes which control scattered sunlight spectra, and define
282 the forward model which is used within iFit to simulate measured spectra.

283

284 Sunlight is the source of radiation in our ultraviolet spectra, and we must therefore
285 take account of the absorption features in the Sun's emission spectrum, known as the
286 Fraunhofer spectrum. In order to do this we use the 2005 FTIR-measured,
287 atmosphere-corrected solar spectrum measured at Mauna Loa, Hawaii, USA reported
288 by Kurucz et al. (<http://kurucz.harvard.edu/sun/fluxatlas2005/>). Some of absorption
289 lines in the Fraunhofer spectrum are strong, practically black, and therefore we did not
290 wish to smooth the spectrum before using it in our forward model, as this would
291 eliminate important features in the final spectrum (this is in fact the source of the I_0
292 effect discussed by Aliwell et al., 2002). However, the Kurucz spectrum is two orders
293 of magnitude high sampling frequency (grid spacing of 0.0013 nm) than our
294 measurement spectrum (0.1 nm grid spacing), causing slow fitting if we perform
295 forward model calculations on the Kurucz wavelength grid. We found by inspection
296 that smoothing the original Kurucz 2005 solar spectrum with an 8 element boxcar and
297 then interpolating onto a forward model grid with 0.01 nm spacing produced identical
298 results as when we used the full Kurucz grid with no smoothing. With a 0.01 nm grid
299 spacing the forward model ran at an acceptable speed on a modern desktop PC.

300

301 Closely related to the solar absorption spectrum is the Ring spectrum (Grainger and
302 Ring, 1962), produced by inelastic molecular scattering. At low SZA's the Ring
303 spectrum can be several percent of the spectrum, and must be accounted for. We use a



304 normalised inverse Kurucz 2005 solar spectrum to produce a Ring spectrum cross-
305 section in the model.

306

307 Absorptions from gas species are accounted for using laboratory measured cross-
308 sections. For all retrievals discussed here we include cross-sections for SO₂ (at 293 K:
309 Bogumil et al., 2003), BrO (at 298 K: Fleischmann et al., 2003; 2004), O₃ (at 223 K:
310 Voigt et al., 2001) and NO₂ (at 223 K: Voigt et al., 2002).

311

312 Wavelength shift and stretch were applied to the forward model, and therefore the
313 forward model was calculated on a wider grid than the measured spectrum grid, with
314 an additional 2 nm added to either end of the fit window limits.

315

316 The forward model calculation proceeds as follows. A model grid is created with 0.01
317 nm grid spacing and an additional 2 nm added at the start and end. The raw Kurucz
318 2005 solar absorption spectrum, smoothed with an 8 element boxcar, is interpolated
319 onto this grid using cubic spline interpolation (this interpolation method is used
320 throughout the forward model calculation). The Ring optical depth is then calculated
321 as the normalised natural log of the interpolated solar spectrum. A Ring amount is
322 multiplied with the Ring optical depth to produce a Ring transmittance. Absorption
323 cross-sections for requested molecular species are also interpolated onto the model
324 grid. The molecular cross-sections are multiplied with gas amounts to produce optical
325 depth spectra for each species. The negative exponential of the optical depths
326 produces transmittance spectra for each gas species. Finally a background polynomial
327 of user-definable order is calculated.

328



329 The solar spectrum, Ring transmittance, gas transmittances and background
330 polynomial are then all multiplied together to produce a raw spectrum, which in
331 theory would be that observed if a perfect, infinitely high resolution spectrometer
332 were used. However, because we are using an imperfect, relatively low resolution
333 spectrometer we must now convolve the high resolution transmittance spectrum with
334 a relatively broad ILS, which is calculated based on a variable resolution parameter
335 and a fixed Gaussian to boxcar weighting (found by inspection). The convolved
336 spectrum is then shifted and stretched onto the measurement spectrum grid. Thus, the
337 measurement itself is never shifted, it is the forward model which adapts to the
338 measurement.

339

340 **4.3 Inclusion of a solar spectrum residual in the forward model**

341

342 During analysis of scattered sunlight spectra we found that the form of the fit residual,
343 $(y-F)/y$, where y is the measurement and F the forward model best fit, had extremely
344 consistent structures, spectrum after spectrum. The cause of these structures was
345 clearly not random noise, but rather the cumulative effect of systematic imperfections
346 in the forward model, with the single greatest error source being the solar spectrum.
347 Given the systematic nature of the residual features it was natural to attempt to
348 average the residual for a few spectra to produce a low-noise residual spectrum and
349 then divide subsequent measurements with the residual spectrum, together with the
350 flat spectrum. This procedure worked well, and produced a quality of fit that was so
351 close to the measurement spectrum that the final residual was pure random noise. We
352 found that the quality of the fit did not degrade as a function of SZA, demonstrating
353 that the main source of the residual features was independent of SZA, confirming the



354 hypothesis that the residual structures were produced by imperfections in the Kurucz
355 solar spectrum.

356

357 The real challenge for iFit was therefore to be able to fit measured spectra with
358 enough accuracy in the absence of a clear sky spectrum that we could obtain good
359 solar spectrum residuals with a minimum of contamination from SO₂. As we show in
360 the case studies this was achieved, with 1-2% fit residuals without using a solar
361 spectrum residual. This limits the magnitude of SO₂ contamination to ~20 ppm.m.

362

363

364 **4.4 Non-linear fitting of the forward model to the measurement**

365

366 All retrieval procedures have two main elements, a forward model and an iterative
367 algorithm which adjusts the parameters of the forward model in an efficient manner to
368 achieve the best possible fit to the measured data. In the previous sections we have
369 discussed the forward model, here we examine the second main element, the retrieval
370 algorithm.

371

372 The approach taken was optimal estimation, which allows errors on both the forward
373 model parameters and the measurement to be combined in a sensible fashion to
374 achieve an optimal result (Rodgers et al., 1976, 2000). We used a version of optimal
375 estimation which utilised a non-linear, variably damped, Levenberg-Marquardt (L-M)
376 algorithm for rapid convergence to the best fit. In the optimal estimation standard
377 terminology the group of forward model parameters fitted in the retrieval is called the
378 state vector (x) and the forward model is a function of the state vector, $F(x)$. The



379 objective of the retrieval is to adjust x until $F(x)=y$, where y is the measurement, in
380 our case a UV intensity spectrum.

381

382 In order to calculate a new x at each iteration the retrieval requires knowledge of
383 dF/dx , the gradient of F as a function of changes in elements of the state vector. This
384 function is called a weighting function or Jacobian and has the symbol K . At each
385 iteration new values for x are calculated using a Newton-Raphson method where
386 $\Delta x=(y-F)/K$, with Δx being the change in the state vector in the next iteration.

387 However, since several of the parameters in the state vector are non-linear with
388 respect to the forward model it is clear that when the forward model is far from the
389 measurement, particularly at the start of the fitting procedure, simply calculating the
390 next x based on an implicitly linear assumption that K is constant will potentially send
391 the state vector far from an improved fit. The L-M formulation of the retrieval
392 includes a damping factor, λ , which reduces how far a jump is made at each
393 iteration. This factor is adjusted at each iteration to either be weaker if the fit is
394 improving or stronger if the new iteration produced a worse result than the previous
395 one, allowing efficient convergence even in highly non-linear systems.

396

397 A new K must be calculated at each iteration when using the L-M approach. We
398 calculate K in a purely empirical fashion, running the forward model n_x times, where
399 n_x is the number of elements of the state vector, and multiplying each individual state
400 vector element by a factor of 1.1 to produce a partial derivative of F as a function of
401 each element of the state vector. The weighting function is then the collected partial
402 derivatives of F as a function of each element of x .

403



404 **4.5 Measurement error and fit errors**

405

406 One of the most powerful and useful aspects of the optimal estimation approach is the
407 accurate, quantitative treatment of errors in the resulting fitted elements of the state
408 vector. The most critical input parameter to the final error attributed to each parameter
409 is the error attributed to each element of the measured spectrum. This is calculated by
410 taking the measured spectrum over the fit window, smoothing it with a 3-element
411 boxcar and subtracting the smoothed spectrum from the original spectrum. The
412 standard deviation of the result is used as an estimate of the noise level of each
413 element of the measured spectrum. The validity of this approach is demonstrated by
414 the similarity between the calculated standard deviation of the fit residual of the
415 highest quality fits and the initial measurement noise determination (see section 5.2).

416

417

418 **5. Test Cases**

419

420 In the following sections we present a series of test cases, where the iFit retrieval is
421 applied to spectra collected in a range of situations, from clear sky spectra, to SO₂
422 calibration cell spectra and finally volcanic plume traverse data. The purpose of these
423 tests is to demonstrate the detection limit and error performance of the iFit system
424 using the basic fit, flat spectrum removal and solar spectrum residual removal. By
425 using the calibration cell spectra we determine the accuracy and precision of iFit.
426 Finally, we use the traverse data test case to demonstrate the efficacy of the retrieval
427 for volcanic plume SO₂ and BrO retrievals.

428



429 In the test cases several instrumental arrangements were used. For the clear sky and
430 calibration cell tests we used two new USB2000+ spectrometers (model names
431 HO7120 and HO7121) with 50 micron slit, grating #7 tuned to 280-400 nm, 2000
432 series detector with UV2 window, L2 detector lens, OF1-U325C bandpass filter, 1000
433 micron diameter solar resistant fibre, and an Ocean Optics 74-UV f/2 10 mm focal
434 length quartz collimating lens, with 5.7° field of view. SO₂ calibration cells were
435 originally within a COSPEC instrument and were placed directly in front of, and
436 perpendicular to, the collimating lenses.

437

438 For the Etna traverse test case a USB2000 spectrometer was used (USB2G1338), with
439 200 micron slit, grating #7 tuned to 280-400 nm, 2000 series detector with UV2
440 window, L2 detector lens, 1000 micron diameter solar resistant fibre, and an Ocean
441 Optics 84-UV f/4 100 mm focal length quartz collimating lens, with 0.57° field of
442 view.

443

444 **5.1 Flat spectra**

445

446 The CCD sensor in the USB2000 spectrometers has a slightly different response for
447 each individual pixel, which can be characterised by measuring a deuterium light
448 source (Ocean Optics DT1000). This produces a spectrum called a flat spectrum,
449 which can be removed from the measured intensity spectrum prior to fitting to
450 improve fit quality. We measured the flat spectra for both our USB2000+
451 spectrometers and the USB2000 spectrometer, using a smoothed flat spectrum to
452 normalise the result. Integration time was 1 ms and 10,000 spectra were coadded to
453 produce each spectrum. We were curious to see if the flat spectrum was temperature



454 dependent, and conducted measurements after the USB2000+ spectrometers were left
455 inside a 3-4°C fridge for 1 hour and in ambient 26°C to examine this question. The
456 results are shown in Figure 1, and show a flat spectrum which is quite different for
457 each spectrometer, with standard deviation of 2-3% and insignificant temperature
458 variability.

459

460 There is an important point to make with regards to the flat spectrum. This spectrum
461 is characteristic of the individual pixels of the CCD, and is therefore not affected by
462 wavelength shifts in the spectrometer: it is absolutely fixed. USB2000 spectrometers
463 exhibit temperature-dependent wavelength shifts, probably due to thermal expansion
464 effects in the chassis. This helps to explain why in a classic DOAS analysis of
465 traverse data collected using a clear sky spectrum the fit may degrade during the
466 course of the traverse, if a non-temperature stabilised spectrometer is used. The
467 radiation spectrum will be shifted relative to the flat spectrum, producing an
468 increasingly significant misfit. This, together with better dark spectrum stability, is
469 one of the main reasons why temperature stabilisation is a good idea, if the flat
470 spectrum is not known. However, it is extremely simple to measure the flat spectrum,
471 and once it is done can probably be used for extended periods of time before the CCD
472 performance changes significantly. Therefore, by accurately characterising the flat
473 spectrum, we avoid the necessity for temperature stabilisation, considerably
474 simplifying the design, energy consumption and use of the spectrometers.

475

476

477 **5.2 Test case 1: Clear sky**

478



479 For our first test case we set up both USB2000+ spectrometers viewing the sky from
480 the Pisa office of INGV on 14 June 2012. We started data collection at 12:20 and
481 ended at 19:00 local time. Integration time was adjusted during the course of the day
482 to maintain optimal intensity levels. Between 12:20 and 14:30 80 msec integration
483 time spectra were co-added 600 times for each measured spectrum which were
484 collected approximately every 42 seconds In this time period the sky was hazy with
485 occasional cumulus clouds. Between 14:30 and 16:05 160 msec integration time
486 spectra were co-added 200 times for each measured spectrum which were collected
487 approximately every 32 seconds. In this time period there was clear blue sky with
488 occasional cumulus clouds. Between 16:05 and the end of measurements 280 msec
489 integration time spectra were co-added 50 times for each measured spectrum which
490 were collected approximately every 14 seconds. In this time period there were white
491 wispy clouds and blue sky, and from 16:30 onwards the sky was clear.

492

493 The FWHM of the ILS was fitted and a Gauss-Boxcar weighting of 0.95:0.05 was
494 used. An order 5 polynomial was fitted together with shift, stretch, O₃, NO₂, SO₂ and
495 Ring. A typical SO₂ fit window of 308-318 nm was used.

496

497 The result of the iFit retrieval applied without removal of the flat spectrum is shown
498 in Figure 2, and demonstrates that even in its most basic form a residual with 2%
499 standard deviation is achieved. Removal of the flat spectrum produces an improved fit,
500 as shown in Figure 3, with a 1% standard deviation of the residual. Removing the
501 solar spectrum residual produces the results shown in Figure 4, with a 0.2% standard
502 deviation of the residual. This fit error is the same as the empirically determined



503 measurement error, indicating that the fit has successfully included all the features of
504 the measured spectrum.

505

506 The fit errors are plotted against empirically-determined measurement error for each
507 of the three fit procedures in Figure 5. The steadily improving performance of the
508 retrieval is clear as first flat and then solar spectrum residual are included. The final fit
509 achieves close to 1:1 performance with the measurement error, confirming the fidelity
510 of iFit.

511

512 Obtaining good zero baseline performance for SO₂ amounts when there is no SO₂
513 present is of critical importance for the iFit retrieval, and this performance is
514 demonstrated in Figure 6. There we present the retrieved SO₂ amounts for each iFit
515 procedure, when there is no SO₂ in the atmosphere. The impact of the flat spectrum is
516 dramatic, significantly improving the performance of the SO₂ retrieved amounts.
517 Removal of the solar spectrum residual produces very high precision results, with a
518 systematic offset from zero which remains within $5e^{16}$ molecules.cm⁻² or 20 ppm.m of
519 zero until dusk. This is more than adequate performance for volcanic applications.

520

521 It is important to note that the performance of the solar spectrum residual does not
522 degrade over the course of the day, other than that produced by the steadily increasing
523 noise of the spectra. This is critically important, because it confirms that the solar
524 spectrum residual is not air mass factor or solar zenith angle dependent, but is instead
525 a product of inaccuracies in the measured solar spectrum.

526

527 **5.3 Test Case 2: Calibration Cell Tests**



528

529 On 15th June 2012 we conducted further measurements using the sky as a source of
530 radiation, but this time using two calibration cells, one containing 126 ppm.m and the
531 other 405 ppm.m SO₂. These cells were measured simultaneously with the two
532 USB2000+ spectrometers during the course of the day from 12:50 until 19:44 local
533 time. Spectrometer HO7120 was used with the 405 ppm.m cell, and measured spectra
534 with 140 ms integration time and 150 co-adds, for a total measurement time of 21
535 seconds for each spectrum. Spectrometer HO7121 was used with the 126 ppm.m cell,
536 and measured spectra with 100 ms integration time and 150 co-adds, for a total
537 measurement time of 15 seconds for each spectrum. Fits using both flat removal and
538 residual removal were performed, using a solar spectrum residual calculated by fitting
539 the SO₂ calibration cell spectra with a flat spectrum. The typical fits for the HO7210
540 spectrometer using flat and solar spectrum residual fitting are shown in Figures 7 and
541 8 respectively. These indicate that the maximum value of SO₂ that could be left in the
542 solar spectrum residual cannot exceed ~1% absorption, equivalent to an SO₂ amount
543 of ~20 ppm.m.

544

545 The stable concentrations in this all-afternoon test allowed us to investigate the ideal
546 SO₂ fit window. We did this by fitting the entire dataset with a range of fit windows,
547 producing a mean and standard deviation for the entire set for each window. The
548 results from this study are shown in Figure 9. We chose an optimal fit window of 308-
549 318 nm, as this produces reasonably accurate results, within 10% of the gas cell
550 amounts, and allows a stronger SO₂ line to be included to increase the sensitivity of
551 the retrieval to small amounts of SO₂. We see that while the accuracy of the fit does
552 change with the fit window, the empirical precision is impressively small, and



553 consistent with retrieved SO₂ errors. This opens the possibility to correct the
554 systematic differences between calibrated SO₂ amounts and retrieved SO₂ amounts.

555

556 We show the time series of SO₂ retrieved values using both solar spectrum residual
557 and flat fits for the dataset up until light decreases to low levels in Figure 10. There is
558 a fairly flat systematic underestimate of ~10% for the 405 ppm.m cell and 10%
559 overestimate in the 126 ppm.m cell. These can be readily corrected. A modest 2-3%
560 decline in SO₂ values is observed during the course of the day. The two retrievals
561 produce near identical results, consistent with small residual of the flat fit.

562

563 **5.4 Test 3: Etna traverse: SO₂**

564

565 Our third test case uses data from an example dataset of spectra collected during a car-
566 based traverse of Mt. Etna, Sicily, Italy on 7th January 2007. This dataset was chosen
567 as the solar radiance in January is relatively low, and therefore represents a close to
568 worst-case scenario. No flat spectrum was measured at the time of the traverse, but we
569 produced one in July 2012 which improved the fit residual when it was removed from
570 the measurement, demonstrating the stability of this feature. The abundant number of
571 clear sky spectra between the plume measurements permitted an accurate
572 determination of the residual solar spectrum with SO₂ fixed to zero. An example fit of
573 an SO₂-rich spectrum is shown in Figure 11, and the retrieved SO₂ time series is
574 shown in Figure 12. Good quality baseline fits and clean SO₂ profiles characterise the
575 SO₂ traverses.

576

577 **5.5 Test 4: Etna traverse: BrO**



578

579 We performed a BrO retrieval using a solar spectrum residual corrected fit, with a
580 window of 337-352 nm, and simultaneously fitting BrO, SO₂, O₃, NO₂ and Ring
581 spectra, as well as an order 4 polynomial, shift, stretch and FWHM of the instrument
582 lineshape. Results from an example spectrum (the same used in Figure 11) are shown
583 in Figure 13. Note the 0.3% residual, equivalent to the measurement error. The BrO
584 time series is shown in Figure 14, showing greater variability than that in the SO₂ due
585 to the relative weakness of the BrO absorption. Retrieved SO₂ values are plotted
586 against BrO values in Figure 15, indicating a strong correlation between the two
587 species and a BrO/SO₂ ratio of 2.4e⁻⁴. Note the consistency of the retrieved errors. We
588 conclude that iFit performs well for both BrO and SO₂ retrievals.

589

590

591 **6. Discussion**

592

593 The main benefits of the iFit approach are that; it allows accurate determination of
594 SO₂ amounts from spectra without the need for collection of a clear sky spectrum; the
595 quality of fit is limited by measurement noise, not the forward model or retrieval
596 procedure; inclusion of the flat spectrum greatly reduces the impact of temperature-
597 dependent wavelength shifts; intensity-based retrievals include the full broadband
598 absorption of SO₂, which can make up more than 50% of the total SO₂ absorption.
599 Intensity-based retrievals also allow direct characterisation of aerosol/ash absorptions
600 and accurate modelling of light dilution effects, and these two aspects will be
601 addressed in future work.

602



603 iFit opens up the possibility for original new approaches to manual and automated
604 SO₂ and BrO retrievals during both traverse and scanning measurements, and
605 potentially removes the necessity for temperature stabilisation of spectrometers.

606

607 We have shown that the residual solar spectrum is not air mass factor dependent,
608 indicating that it is the result of inaccuracies in the solar spectrum. Errors at the 1-2%
609 level are not surprising for atmospheric corrected solar spectra, but the key capability
610 of the iFit code to accurately fit the main gas absorptions until the 1-2% solar
611 spectrum error limit is reached means that the residual spectrum is an essentially pure
612 solar spectrum correction function. This can then, in theory, be re-applied independent
613 of solar zenith angle, air mass factor, weather conditions, and so on. To date all of our
614 tests have supported this capability.

615

616 The flat spectrum is pixel dependent, and will not shift with temperature induced
617 wavelength shifts. By accurately characterising the flat spectrum we may elegantly
618 remove its effects on the measured spectrum, making the resulting spectra robust to
619 wavelength shifts, which may be accurately fitted in the iFit procedure. Using the flat
620 spectrum removal procedure to produce a residual which is in turn removed allows
621 iFit to produce noise-limited fits of SO₂ and BrO for traverse data.

622

623 Scanning data requires a slightly more complex approach. Here we may produce a
624 stored residual solar spectrum for each spectrometer, which is then applied to all fits,
625 taking account of any shifts between the measured residual and the current fit
626 spectrum. Alternatively, and perhaps more robustly, we may use the capability of the
627 flat-equipped fit to produce a 1-2% solar spectrum residual by fitting the vertical



628 viewing spectrum in a single scan. The elegance of this approach is that we account
629 for nearly all SO₂ (down to at most 10-20 ppm.m) which may be present, as opposed
630 to the classic DOAS clear-sky spectrum method, which introduces unknown
631 magnitude biases into the scan retrieval. The iFit procedure may then perform a solar
632 spectrum residual-corrected fit, achieving optimal quality results, scan by scan.

633

634 We may apply this approach to automated BrO fitting of scan data. BrO fitting is a
635 challenge without a solar spectrum residual-corrected fit in iFit, because the 1-2%
636 variability is much higher than the BrO absorption. It is therefore difficult to produce
637 a BrO-free residual, because while BrO could be fixed to zero in the fit if there is
638 volcanic gas present then there will be a systematic offset, the same problem DOAS
639 has for SO₂. There are two solutions to this. Firstly, using the SO₂ amount retrieved
640 from the vertical spectrum in a scan we may apply the mean SO₂/BrO ratio to fix the
641 BrO content when fitting the vertical spectrum in the BrO window, producing a
642 residual solar spectrum with little if any BrO. The residual solar spectrum may then be
643 used throughout the scan to produce a BrO profile. Secondly, we may simply ignore
644 the fact there is a potential bias in the BrO profile. The SO₂/BrO ratio will be
645 determined by plotting SO₂ amounts against BrO and calculating the gradient of the
646 plot using linear regression. In this case any bias in BrO has no effect on the SO₂/BrO
647 ratio; indeed, the intercept of the regression will reveal the magnitude of the BrO bias.

648

649 The iFit approach is therefore ideally suited to the automatic analysis of spectra
650 produced by automatic scanning networks. We will be shortly implementing iFit for
651 the FLAME scanning UV networks on Etna and Stromboli, and propose that iFit be
652 also applied to other networks of UV scanning systems.



653

654 The background polynomial produced during the iFit procedure is the multiplication
655 of the source intensity with the aerosol absorptions in the atmosphere and plume. By
656 dividing the polynomial produced in an SO₂-rich spectrum with one in a clear sky
657 spectrum we produce a pure plume aerosol/ash transmittance spectrum that may be
658 used to accurately characterise interference in measurements made by the SO₂ camera.
659 This information is challenging to produce from the classic DOAS fit, as the
660 broadband absorptions of O₃ and SO₂ are lost. In theory they could be recalculated,
661 but at that point the retrieval is effectively reproducing an intensity fit, which perhaps
662 makes more sense to perform directly, as is the case for iFit.

663

664

665 7. Conclusions

666

667 iFit is a new intensity-based retrieval algorithm for direct fitting of measured UV
668 spectra, specifically developed for use in volcanology. It has been designed with a
669 focus on minimising processing of the measured spectra prior to analysis. Here, we
670 report a detailed presentation of the iFit algorithm, and test it in 4 case studies,
671 examining clear sky spectra, SO₂ calibration cell experiments and volcanic SO₂ and
672 BrO retrievals from traverse measurements performed on Mt. Etna volcano, Italy. It
673 can be robustly and easily applied to both scanning and traverse measurements of
674 volcanic plumes, producing bias-free profiles of SO₂, and accurate SO₂/BrO ratios
675 without the need for clear sky background spectra. Fit residuals are typically pure
676 instrumental noise when the residual solar spectrum is removed.

677



678 We have shown that the major source of fit error in the intensity fitting come from the
679 AMF-independent solar spectrum errors, which are however easily characterised and
680 removed. Furthermore, we have quantified the magnitude of the flat spectrum in three
681 spectrometers, and shown that this spectrum is strongly spectrometer dependent but
682 temperature independent, opening the possibility for robust analysis and
683 quantification of both SO₂ and BrO without the need for temperature stabilisation.

684

685 The iFit procedure calculates the full SO₂ and O₃ spectra, including their significant
686 broadband components. We can therefore easily characterise the aerosol/ash
687 transmittance spectrum allowing much improved corrections to SO₂ camera data. The
688 intensity-based approach also opens the possibility to directly fit light dilution effects.
689 Both of these subjects will be the focus of future work.

690

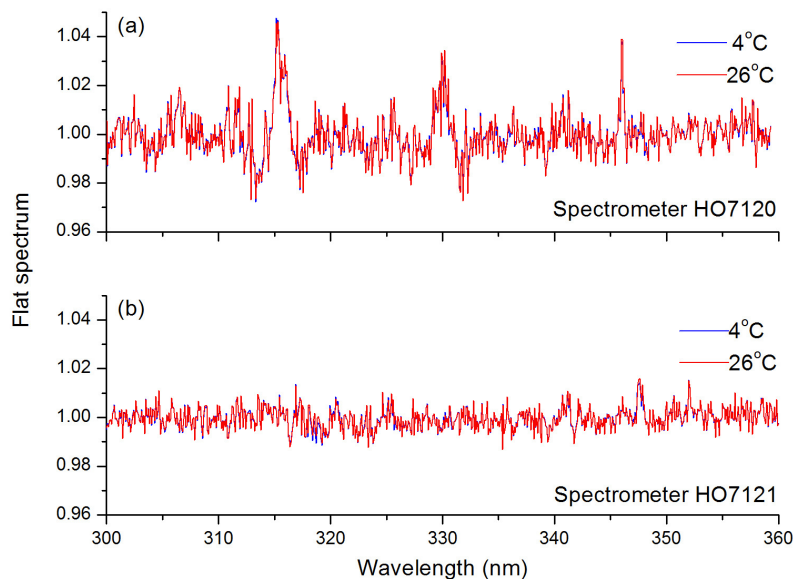
691 **Acknowledgements**

692

693 This work was produced with support from ERC grant CO₂Volc, StG 279802 (P.I.
694 Mike Burton, INGV Pisa). GS was supported through a grant from Region
695 d'Auvergne Chaire d'Excellence (P.I. Andrew Harris, LMV, Clermont Ferrand,
696 France), and this paper represents CLERVOLC contribution 001. The work reported
697 here was produced during a visit by GS to INGV Pisa, for which we acknowledge the
698 support of A. Neri, R. Rapuzzi and L. Nannipieri. We gratefully acknowledge fruitful
699 discussions with Christoph Kern and Vitcho Tsanev and instrumental support from
700 Giuseppe Salerno.

701

702

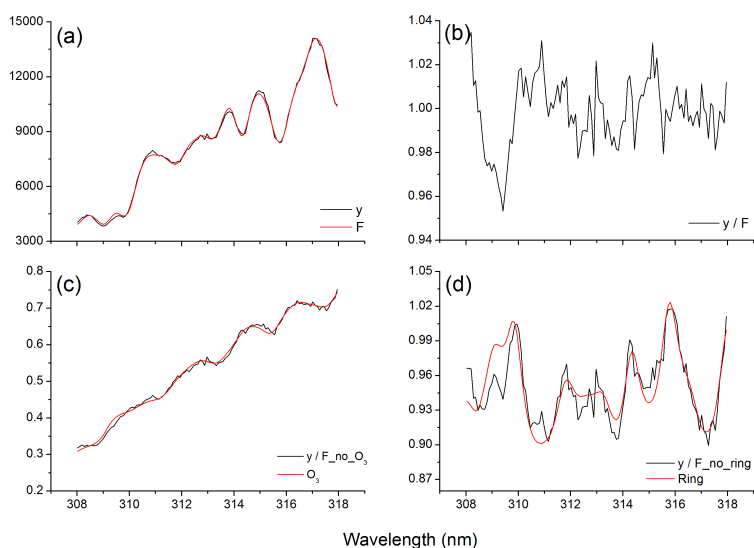


703

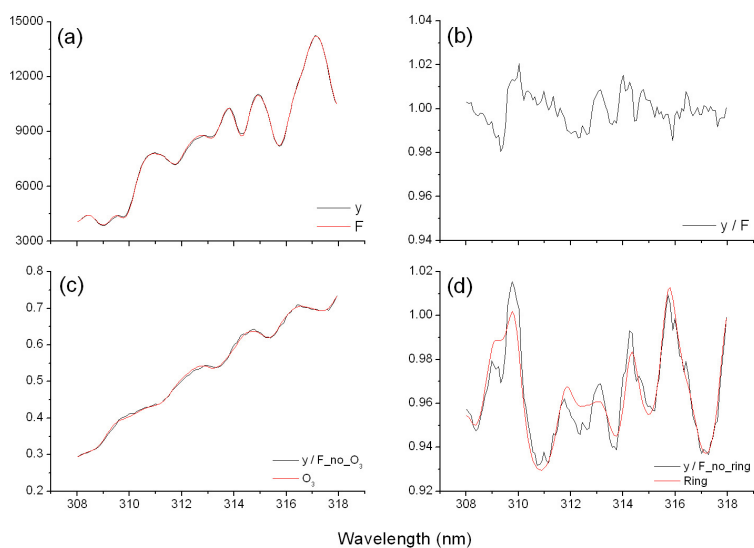
704 Figure 1. Flat spectra for USB2000+ spectrometers collected with a deuterium lamp
705 and normalised with boxcar smoothed spectra, at 26°C and 4°C. Note that the
706 behaviour of the two spectrometers is quite different, with HO7120 exhibiting
707 significantly greater variability than HO7121. No significant difference in the flat
708 spectra was observed with a 22°C temperature variation.

709

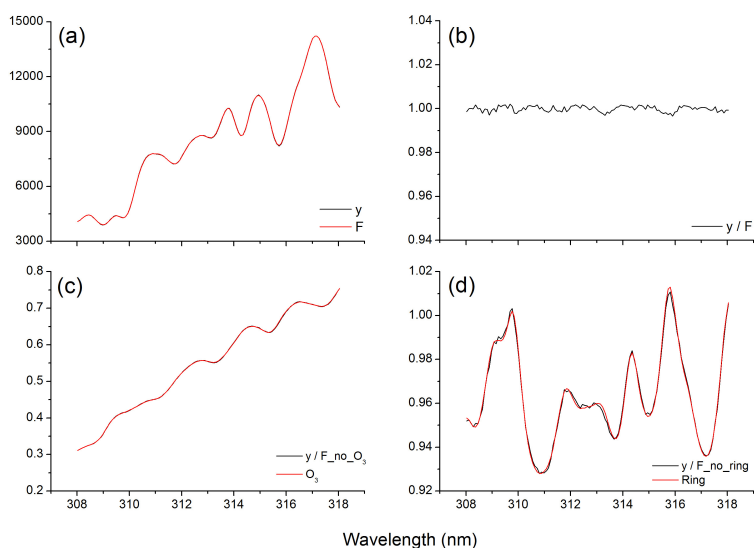
710



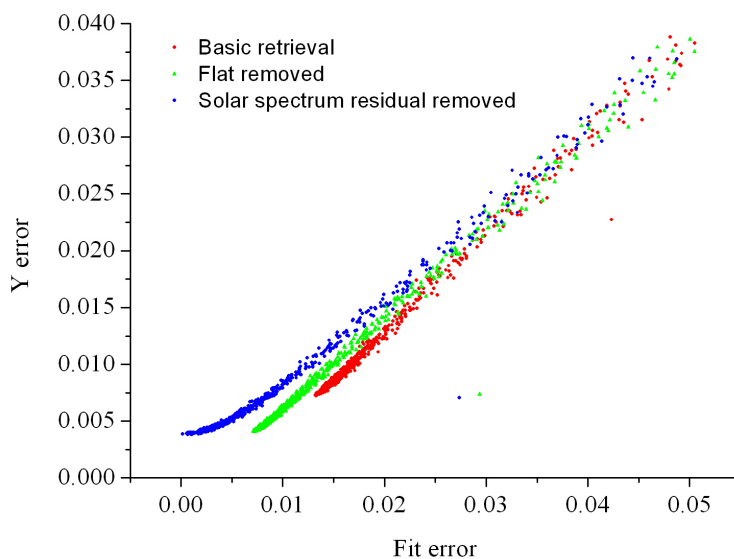
711
712 Figure 2. Examples of an iFit analysis of a clear sky spectrum with no flat spectrum
713 removal. In (a) the measured spectrum and fit are shown in black and red respectively,
714 note the intensity scale. In (b) the residual of the measurement (y) and the fit (F) is
715 shown, calculated as y/F . In (c) the measured spectrum divided by a model calculated
716 spectrum of the best fit without O_3 is shown, together with the fitted O_3 spectrum. In
717 (d) the measured spectrum divided by a model calculated spectrum of the best fit
718 without the Ring spectrum is shown, together with the fitted Ring spectrum.
719
720



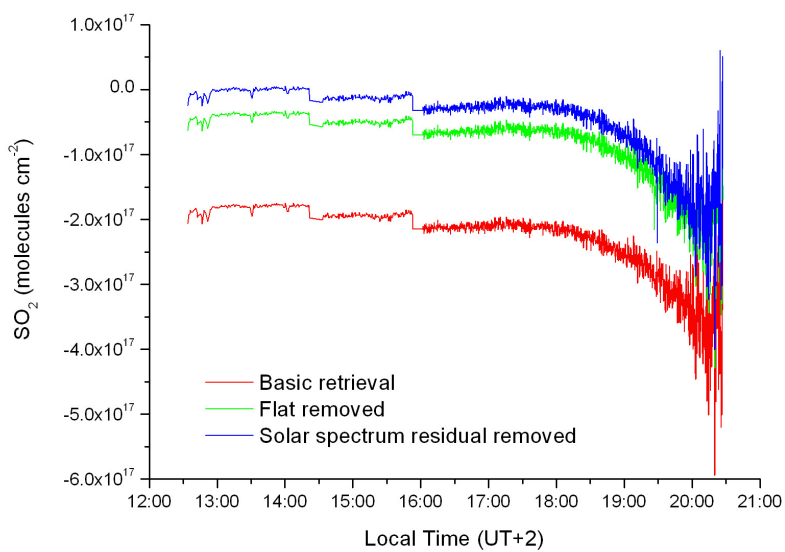
721
722 Figure 3. Examples of an iFit analysis of a clear sky spectrum with flat spectrum
723 removed. In (a) the measured spectrum and fit are shown in black and red respectively,
724 note the intensity scale. In (b) the residual of the measurement (y) and the fit (F) is
725 shown, calculated as y/F . In (c) the measured spectrum divided by a model calculated
726 spectrum of the best fit without O_3 is shown, together with the fitted O_3 spectrum. In
727 (d) the measured spectrum divided by a model calculated spectrum of the best fit
728 without the Ring spectrum is shown, together with the fitted Ring spectrum.
729



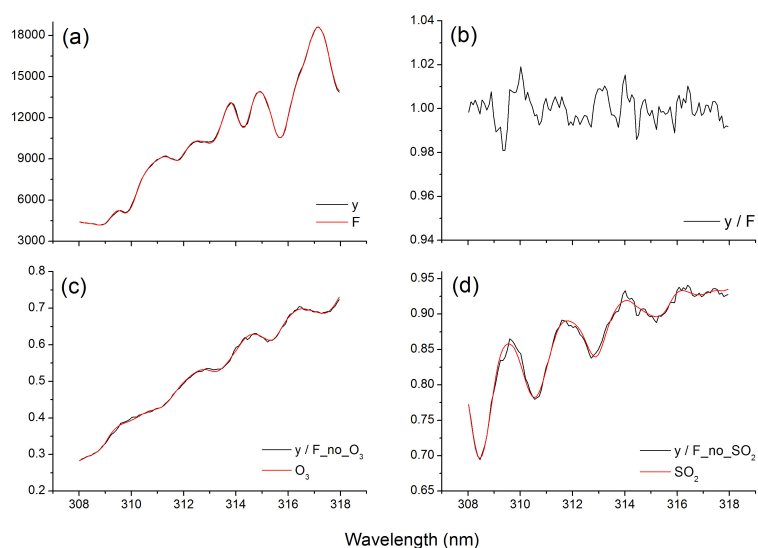
730
731 Figure 4. Examples of an iFit analysis of a clear sky spectrum with solar spectrum
732 residual removed. In (a) the measured spectrum and fit are shown in black and red
733 respectively, note the intensity scale. In (b) the residual of the measurement (y) and
734 the fit (F) is shown, calculated as y/F . In (c) the measured spectrum divided by a
735 model calculated spectrum of the best fit without O_3 is shown, together with the fitted
736 O_3 spectrum. In (d) the measured spectrum divided by a model calculated spectrum of
737 the best fit without the Ring spectrum is shown, together with the fitted Ring
738 spectrum.
739



740
741 Figure 5. Errors produced by the iFit procedure for each spectrum during the 14th June
742 clear sky test using the basic retrieval (red), retrieval with flat spectrum removed
743 (green) and solar spectrum residual removed (blue). The fit error is calculated as the
744 standard deviation of $((F-y)/y)$, where F is the fit and y is the measured spectrum. The
745 y error is calculated by taking the standard deviation of the ratio of the measured
746 spectrum with a 3-element boxcar smoothed version of the measured spectrum.
747



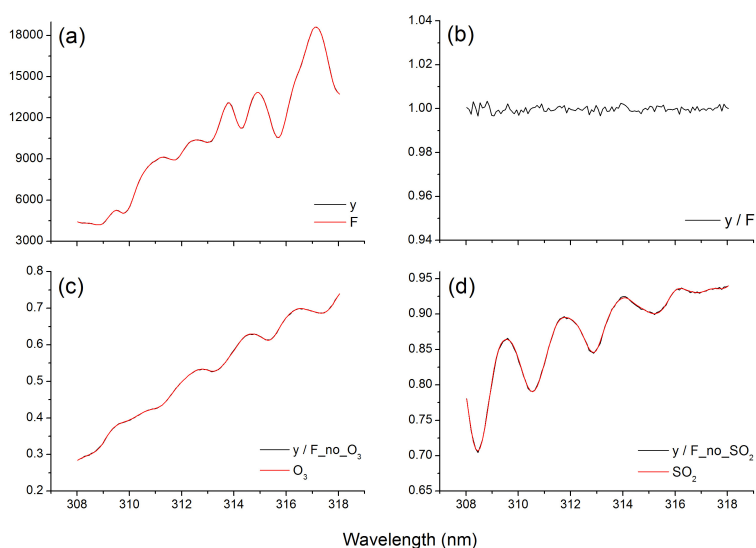
748
749 Figure 6. Retrieved SO₂ time series for three iFit retrievals during the 14th June clear
750 sky test.
751



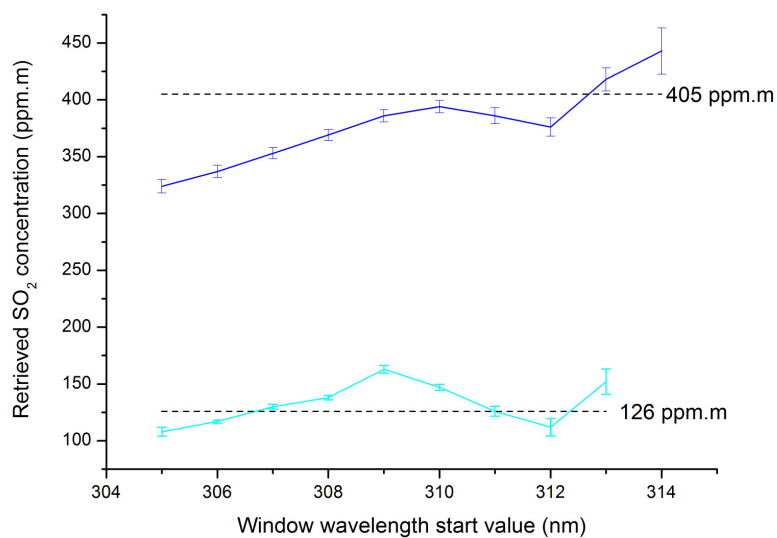
752
753 Figure 7. Example of a fit to a single spectrum with flat spectrum removed, collected
754 with the HO7120 spectrometer on 15th June using the 405 ppm.m calibration cell and
755 sky illumination. In (a) the measured spectrum and fit are shown in black and red
756 respectively, note the intensity scale. In (b) the residual of the measurement (y) and
757 the fit (F) is shown, calculated as y/F . In (c) the measured spectrum divided by a
758 model calculated spectrum of the best fit without O_3 is shown, together with the fitted
759 O_3 spectrum. In (d) the measured spectrum divided by a model calculated spectrum of
760 the best fit without the SO_2 spectrum is shown, together with the fitted SO_2 spectrum.
761 Note the ~1 % residual.

762

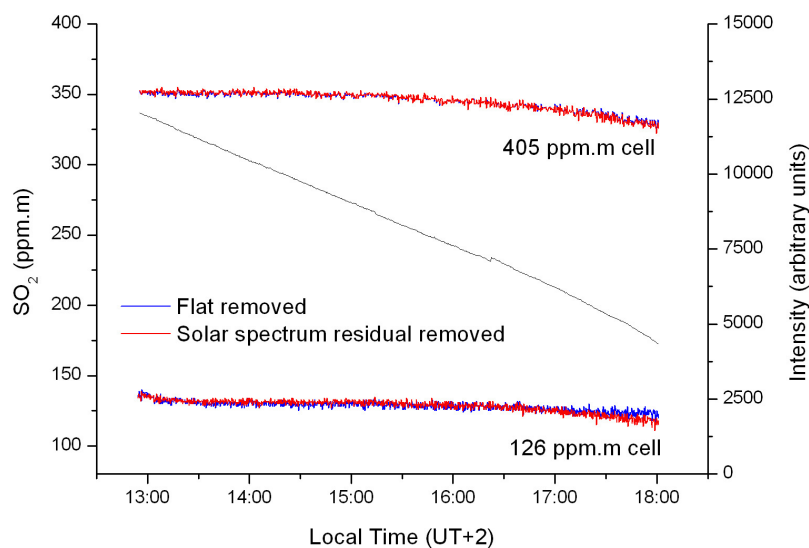
763



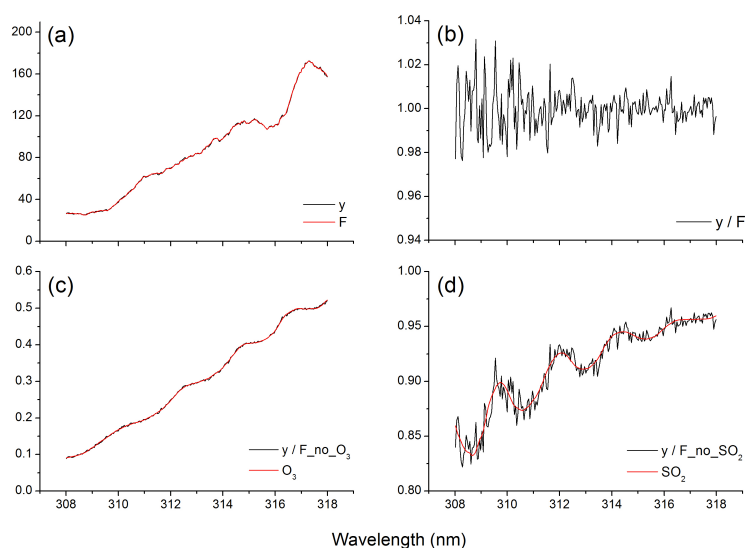
764
765 Figure 8. Example of a fit to a single spectrum with solar spectrum residual removed,
766 collected with the HO7120 spectrometer on 15th June using the 405 ppm.m calibration
767 cell and sky illumination. In (a) the measured spectrum and fit are shown in black and
768 red respectively, note the intensity scale. In (b) the residual of the measurement (y)
769 and the fit (F) is shown, calculated as y/F . In (c) the measured spectrum divided by a
770 model calculated spectrum of the best fit without O_3 is shown, together with the fitted
771 O_3 spectrum. In (d) the measured spectrum divided by a model calculated spectrum of
772 the best fit without the SO_2 spectrum is shown, together with the fitted SO_2 spectrum.
773 Note the 0.2 % residual.
774
775



776
777 Figure 9. Results from an investigation into the effect of fit window on retrieved SO₂
778 amounts with flat removed for both the 405 and 126 ppm.m calibration cells. The
779 window size was fixed at 10 nm. Each point represents the mean value of retrieved
780 SO₂ for the entire dataset up until 6 pm, and the error bar is the ±1 standard deviation
781 of the retrieved SO₂ values.
782

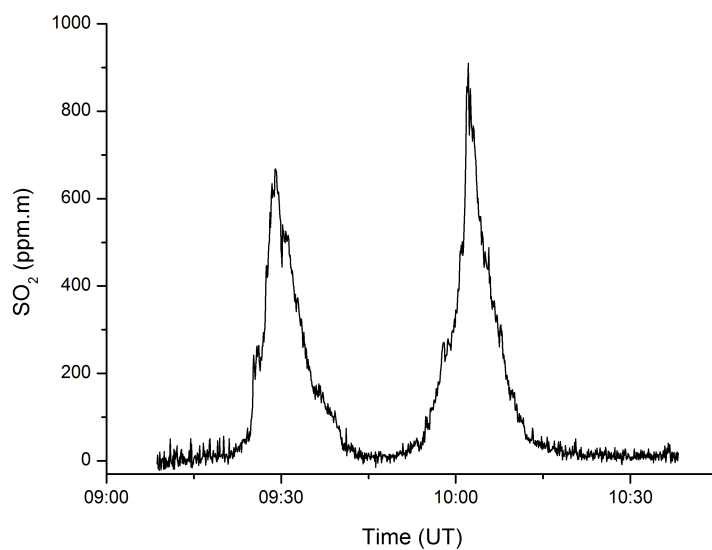


783
784 Figure 10. Retrieved SO₂ time series using the 308-318 nm fit window and both flat-
785 removed and solar spectrum residual-removed fits, for both the 126 ppm.m 405
786 ppm.m cells. Note that systematic differences between stated and measured
787 calibration cell SO₂ concentration-pathlengths arise from minor leakage from the 10
788 year old calibrations cells. Measured intensity is shown as a black line.
789



790
791 Figure 11. Example of a solar spectrum residual-removed fit to an SO₂-rich spectrum
792 (215 ppm.m) collected during a car traverse under the volcanic plume produced by Mt.
793 Etna on 7th January 2007. In (a) the measured spectrum and fit are shown in black and
794 red respectively, note the intensity scale. In (b) the residual of the measurement (y)
795 and the fit (F) is shown, calculated as y/F . In (c) the measured spectrum divided by a
796 model calculated spectrum of the best fit without O₃ is shown, together with the fitted
797 O₃ spectrum. In (d) the measured spectrum divided by a model calculated spectrum of
798 the best fit without the SO₂ spectrum is shown, together with the fitted SO₂ spectrum.
799 Measurement error and fit error were both 0.6 %, indicating that the fit residual is
800 pure instrumental noise.

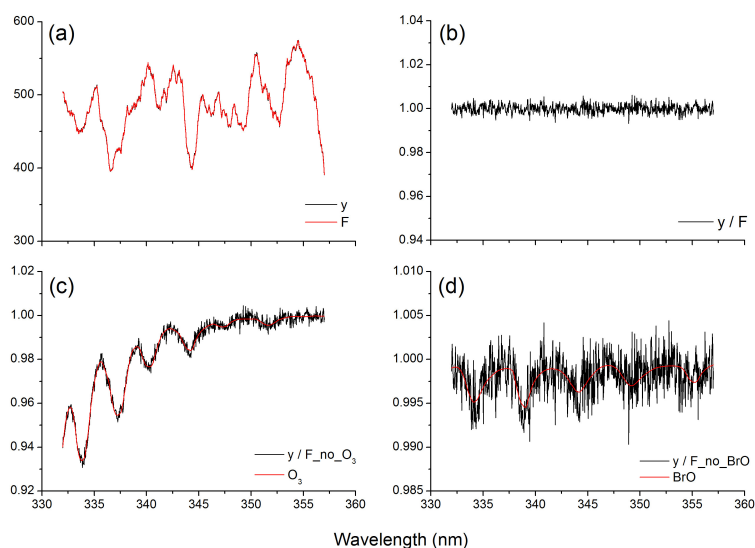
801
802
803
804



805
806 Figure 12. SO₂ time series from a car traverse under Mt. Etna plume on 7th January
807 2007, retrieved with a solar spectrum residual-removed fit.

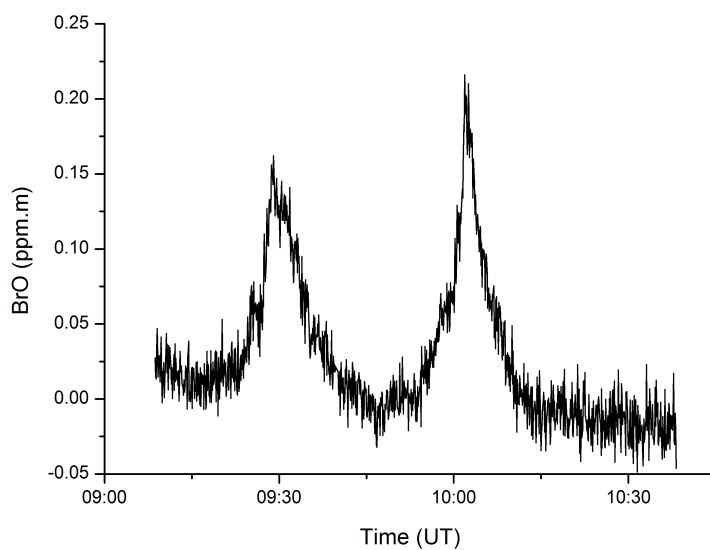
808

809



810
811 Figure 13. Example of a solar spectrum residual-removed fit to a BrO-rich spectrum
812 collected during a car traverse under the volcanic plume produced by Mt. Etna on 7th
813 January 2007. In (a) the measured spectrum and fit are shown in black and red
814 respectively, note the intensity scale. In (b) the residual of the measurement (y) and
815 the fit (F) is shown, calculated as y/F . In (c) the measured spectrum divided by a
816 model calculated spectrum of the best fit without O_3 is shown, together with the fitted
817 O_3 spectrum. In (d) the measured spectrum divided by a model calculated spectrum of
818 the best fit without the BrO spectrum is shown, together with the fitted BrO spectrum.
819 Measurement error and fit error were both 0.3 %, indicating that the fit residual is
820 pure instrumental noise.

821
822
823
824

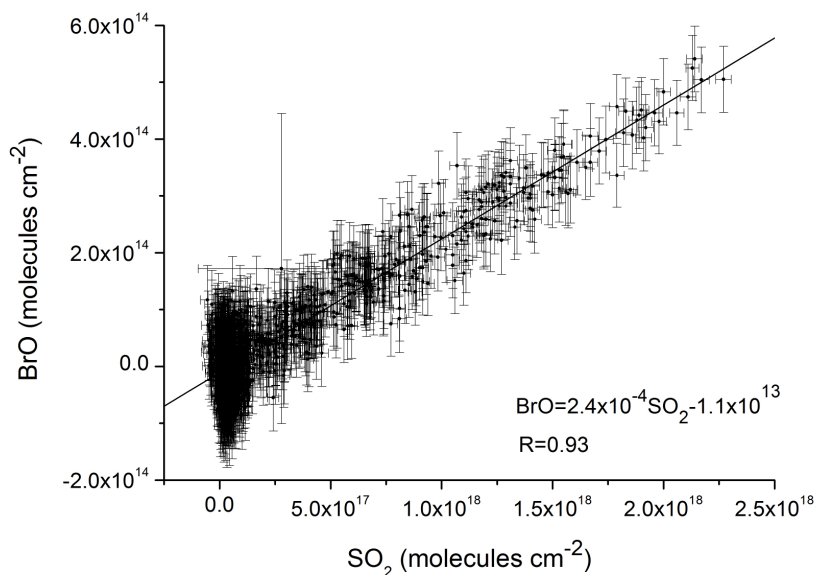


825
826 Figure 14. BrO time series from a car traverse under Mt. Etna plume on 7th January

827 2007, retrieved with a residual-removed fit.

828

829



830

831 Figure 15. SO₂ plotted against BrO for each spectrum of the 7th January 2007 Etna

832 traverse. Error bars are ±1 standard deviations from the retrieval.

833

834



835 References

836

837 Aliwell, S.R., M. Van Roozendael, P.V. Johnston, A. Richter, T. Wagner, D.W.

838 Arlander, J.P. Burrows, D.J. Fish, R.L. Jones, K.K. Tornkvist, J.C. Lambert, K.

839 Pfeilsticker, I. Pundt (2002), Analysis for BrO in zenith-sky spectra: An

840 intercomparison exercise for analysis improvement. *J. Geophys. Res. Atm.*, Vol 107,

841 D14, doi: 10.1029/2001JD000329

842

843 Andres R.J. and Kasgnoc A.D. (1998), A time-averaged inventory of subaerial

844 volcanic sulphur emissions, *J. Geophys. Res.*, 103, D19, 25251-25261.

845

846 Bobrowski, N., Hönninger, G., Galle, B. and U. Platt (2003), Detection of Bromine

847 Monoxide in a Volcanic Plume, *Nature*, 423, 273-276.

848

849 Bogumil, K., J. Orphal, T. Homann, S. Voigt, P. Spietz, O.C. Fleischmann, A. Vogel,

850 M. Hartmann, H. Kromminga, H. Bovensmann, J. Frerick and J.P. Burrows (2003),

851 Measurements of molecular absorption spectra with the SCIAMACHY pre-flight

852 model: instrument characterization and reference data for atmospheric remote-sensing

853 in the 230–2380 nm region. *J. Photoch. Photobio. A*, 157 (2–3), 167–184.

854

855 Burton, M.R., T. Caltabiano, F. Mure, G. Salerno, D. Randazzo (2009) SO₂ flux from

856 Stromboli during the 2007 eruption: Results from the FLAME network and traverse

857 measurements. *J. Volcanol. Geotherm. Res.*, 182 (3-4), 214-220, doi:

858 10.1016/j.jvolgeores.2008.11.025.

859



860 Edmonds, M., R.A. Herd, B. Galle, C.M. Oppenheimer (2003), Automated, high
861 time-resolution measurements of SO₂ flux at Soufriere Hills Volcano, Montserrat.
862 *Bull. Volc.*, 65(8), 578-586, doi: 10.1007/s00445-003-0286-x.

863

864 Fleischmann, O.C., J.P. Burrows, and J. Orphal (2003). Time-windowing Fourier
865 transform absorption spectroscopy for flash photolysis investigations. *J. Photochem.*
866 *Photobiol. A.: Chem.*, 157, 127–136.

867

868 Fleischmann, O.C., M. Hartmann, J.P. Burrows, and J. Orphal (2004). New ultraviolet
869 absorption cross-sections of BrO at atmospheric temperatures measured by a time-
870 windowing Fourier transform spectroscopy. *J. Photochem. Photobiol. A.: Chem.*, 168,
871 117–132.

872

873 Galle, B., Oppenheimer, C. Geyer, A. McGonigle, A.J.S., Edmonds, M., Horrocks,
874 L.A. A miniaturised UV spectrometer for remote sensing of SO₂ fluxes: a new tool
875 for volcano surveillance. *J. Volcanol. Geotherm. Res.* 2003, 119, 241-254.

876

877 Grainger, J.F., J. Ring (1962). Anomalous Fraunhofer line profiles. *Nature*, 193: pp
878 762.

879

880 Galle, B. M. Johansson, C. Rivera, Y. Zhang, M. Kihlman, C. Kern, T. Lehmann, U.
881 Platt, S. Arellano, S. Hidalgo (2010), Network for Observation of Volcanic and
882 Atmospheric Change (NOVAC)-A global network for volcanic gas monitoring:
883 Network layout and instrument description. *J. Geophys. Res. Atm.*, 115, D05304, doi:
884 10.1029/2009JD011823.



885

886 Kantzas, E.P., A.J.S. McGonigle, G. Tamburello, R.G. Bryant (2012) UVolc: A
887 software platform for measuring volcanic SO₂ fluxes. *Computers and Geosciences*, 40,
888 194-199, doi: 10.1016/j.cageo.2011.07.011.

889

890 Platt, U. and Stutz, J. (2008), *Differential Optical Absorption Spectroscopy –*
891 *Principles and Applications*. Springer, Berlin, pp 1–597.

892

893 Rodgers, C.D. (1976), Retrieval of atmospheric temperature and composition from
894 remote measurement of thermal radiation. *Rev. Geophys. Space Phys.*, 14, 609-624.

895

896 Rodgers, C.D. (2000), *Inverse Methods For Atmospheric Sounding, Theory and*
897 *Practice, Series on Atmospheric, Oceanic and Planetary Physics – Vol. 2*, edited by
898 F.W. Taylor, World Scientific.

899

900 Salerno, G.G. M.R. Burton, C. Oppenheimer, T. Caltabiano, V.I. Tsanev, N. Bruno
901 (2009a), Novel retrieval of volcanic SO₂ abundance from ultraviolet spectra. *J.*
902 *Volcanol. Geotherm. Res.*, 181(1-2), 141-153, doi: 10.1016/j.jvolgeores.2009.01.009.

903

904 Salerno G.G., M.R. Burton, C. Oppenheimer, T. Caltabiano, D. Randazzo, N. Bruno,
905 V. Longo (2009b), Three-years of SO₂ flux measurements of Mt. Etna using an
906 automated UV scanner array: Comparison with conventional traverses and
907 uncertainties in flux retrieval. *J. Volcanol. Geotherm. Res.*, 183 (1-2), 76-83, doi:
908 10.1016/j.jvolgeores.2009.02.013.

909



- 910 Stoiber R.E. and Jepsen A. (1973), Sulfur dioxide contributions to the atmosphere by
911 volcanoes, *Science*, 577-578, 182.
912
- 913 Van Roozendael, M., et al. (2012), Sixteen years of GOME/ERS-2 total ozone data:
914 The new direct-fitting GOME Data Processor (GDP) version 5—Algorithm
915 description, *J. Geophys. Res.*, 117, D03305, doi:10.1029/2011JD016471.
916
- 917 Voigt, S., J. Orphal, K. Bogumil and J.P. Burrows (2001), The temperature
918 dependence (203–293 K) of the absorption cross sections of O₃ in the 230–850 nm
919 region measured by Fourier-transform spectroscopy. *J Photochem. Photobiol., A*
920 *Chem.* 143 (1), 1–9.
921
- 922 Voigt, S., J.Orphal and J.P. Burrows (2002), The temperature and pressure
923 dependence of the absorption cross sections of NO₂ in the 250–800 nm region
924 measured by Fourier-transform spectroscopy. *J Photochem. Photobiol., A Chem.*, 149
925 (1–3), 1–7.
926